Geophysical Research Letters

RESEARCH LETTER
10.1029/2021GL094649

Temperature-Dependence of the Clear-Sky Feedback in Radiative-Convective Equilibrium

Lukas Kluft[1,2,3], Sally Dacie[1,2], Manfred Brath[3], Stefan A. Buehler[3], and Bjorn Stevens[1]

[1]Max Planck Institute for Meteorology, Hamburg, Germany, [2]International Max Planck Research School for Earth System Modeling, Hamburg, Germany, [3]Centrum für Erdsystem- und Nachhaltigkeitsforschung (CEN), Fachbereich Erdsystemwissenschaften, Meteorologisches Institut, Universität Hamburg, Hamburg, Germany

Key Points:

- The (negative) clear-sky radiative feedback monotonically increases for surface temperatures between 280 and 330 K
- Masking effects by water-vapor at the flanks of the CO_2 band weaken the radiative forcing at high column water vapor
- At present-day CO_2 concentrations Earth's climate is stable for surface temperatures up to at least 330 K

Supporting Information:

Supporting Information may be found in the online version of this article.

Correspondence to:

L. Kluft,
lukas.kluft@mpimet.mpg.de

Citation:

Kluft, L., Dacie, S., Brath, M., Buehler, S. A., & Stevens, B. (2021). Temperature-dependence of the clear-sky feedback in radiative-convective equilibrium. *Geophysical Research Letters*, *48*, e2021GL094649. https://doi.org/10.1029/2021GL094649

Received 26 FEB 2021
Accepted 29 OCT 2021

Abstract We quantify the temperature-dependence of the clear-sky climate sensitivity in a one-dimensional radiative-convective equilibrium model. The atmosphere is adjusted to fixed surface temperatures between 280 and 330 K while preserving other boundary conditions in particular the relative humidity and the CO_2 concentration. We show that an out-of-bounds usage of the radiation scheme rapid radiative transfer model for GCMs (RRTMG) can lead to an erroneous decrease of the feedback parameter and an associated "bump" in climate sensitivity as found in other modeling studies. Using a line-by-line radiative transfer model, we find no evidence for a strengthening of the longwave radiative feedback for surface temperatures between 305 and 320 K. However, the line-by-line simulations also show a slight decrease in climate sensitivity when surface temperatures exceed 310 K. This decrease is caused by water-vapor masking the radiative forcing at the flanks of the CO_2 absorption band, which reduces the total radiative forcing by about 18%.

Plain Language Summary The climate feedback parameter describes how the net radiative balance at the top of the atmosphere changes with surface temperature. The magnitude of the feedback parameter here depends on the current state of the climate system. For example, a warmer climate state is accompanied by a moister atmosphere which limits the climate feedback and hence increase climate sensitivity—which is the surface warming due to a doubling of CO_2. Other modeling studies have shown that the climate sensitivity will first increase in a warmer reference climate, but decrease again when surface temperatures exceed 310 K. In this study, we are using a reference radiative transfer model to show how the misuse of a simplified radiation scheme can lead to this spurious signal in the estimation of the climate feedback parameter. In addition, we explain how changes in the H_2O and CO_2 concentrations influence the spectral distribution of both the feedback parameter and the radiative forcing.

1. Introduction

The state-dependence of the climate sensitivity is of great interest when studying climate change as it influences the interpretation of the proxy record (Kutzbach et al., 2013; Manabe & Bryan, 1985), historical temperature observations (Andrews, 2014; Gregory & Andrews, 2016), and the interpretation of differences among models (Bourdin et al., 2021). Recent modeling studies, ranging from conceptual (Meraner et al., 2013) to cloud-resolving models (Romps, 2020), find that after an initial decrease the magnitude of the clear-sky feedback parameter, λ, again increases at yet higher surface temperatures (T_s). This non-monotonicity manifests itself as a pronounced "bump," a maximum in the clear-sky climate sensitivity, S, at $T_s \approx 310$ K. Some studies (e.g., Popp et al., 2016; Schneider et al., 2019; Wolf & Toon, 2015) detect different cloud mechanisms that may cause a local maximum in climate sensitivity. In this study, however, we focus on the growing but still inconclusive literature on the seemingly simpler question of the clear-sky radiative response to warming.

Seeley and Jeevanjee (2021) describe a physical mechanism that explains the changing temperature-dependence of λ: when the rise of the temperature is tied to the rise of CO_2, the increased CO_2 concentration broadens the spectral interval over which CO_2 is the dominant absorber, thereby coupling the outgoing-longwave radiation (OLR) in these spectral regions to the tropospheric temperature, and hence T_s in a way that leads to a more negative λ with warming. The work by Seeley and Jeevanjee (2021) provides an elegant physical explanation for the climate sensitivity "bump" in studies with varying CO_2 concentration

(e.g., Romps, 2020) and in doing so shows how λ effectively depends on CO_2. However, their mechanism fails to explain a similar "bump" in S as temperature increases in constant-CO_2 simulations as in Meraner et al. (2013). Moreover, coupling temperature changes to CO_2, while physical, makes it difficult to separate the state-dependence of λ on T_s from its dependence on CO_2.

In this study, we calculate S as a function of a fixed T_s, for $T_s \in [280\ K, 330\ K]$. After the atmosphere has equilibrated to the boundary conditions and the chosen T_s, the radiative feedback is computed as the change in OLR between simulations at increasing T_s (Section 2). Calculations were initially performed using a fast radiative transfer model (Mlawer et al., 1997), identical to that used in many climate modeling studies. To check the calculations of the more parameterized fast radiative transfer model, and to understand how the spectral forcing and feedback associated with a doubling of atmospheric CO_2 depends on temperature, we also perform calculations with a line-by-line model. We find that qualitative errors from the fast radiative model become pronounced as T_s increases above 300 K, and it overestimates the temperature-dependence of S by more than a factor of two as compared to the line-by-line model reference (Section 3).

Studies of the clear-sky feedback date back to Simpson (1928), who proposed that—in an atmosphere whose optical properties arise from a condensible species (water)—OLR decouples from T_s when the atmosphere becomes optically thick. Ingram (2010) brought these ideas to the attention of the climate community (in the meantime planetary scientists, initially unaware of Simpson's work, had come to similar conclusions) and concluded that if the water vapor concentration is a function of temperature only, a warming atmosphere will increases its optical thickness (and hence its emission height) in a way to maintain a constant emission temperature. For Earth's atmosphere this happens when $T_s > 300$ K (Goldblatt et al., 2013; Koll & Cronin, 2018). This decoupling was later (and independently) shown to underpin a limit to how much energy Earth's troposphere can radiate to space in the thermal infrared (Nakajima et al., 1992), with runaway (greenhouse) warming ensuing when the absorbed insolation exceeds this limit (Goldblatt et al., 2013, 2017; Kasting, 1988; Nakajima et al., 1992). These findings encourage the expectation that λ and hence S will increase monotonically with T_s, increasingly so for $T_s > 310$ K, rather than to first increase and then decrease, as found by Meraner et al. (2013). Our line-by-line calculations support the conceptual idea of an increasing feedback: beyond a small local plateau, λ continues to increase monotonically with warming. Using the spectral information of our line-by-line simulations we show that this is not only driven by the rapid closing of the atmospheric emission window, but also by water-vapor becoming the dominant absorption species at the flanks of the CO_2 bands. By considering the spectral response to warming and forcing (Section 4) we are able to understand this behavior, also in light of the earlier literature.

2. Methods and Data

To analyze how the clear-sky climate sensitivity, S, varies with surface temperature, T_s, we use the one-dimensional radiative convective equilibrium (RCE) model konrad (Dacie et al., 2019; Kluft et al., 2019). The representation of the climate system, or even just the climate of the tropics, in terms of cloud (as well as aerosol and ozone) free RCE is a strong, but common, simplification. The Charney et al. (1979) report took it as a starting point and a large body of literature since then has found RCE solutions to be informative of how different physical processes influence climate sensitivity. For this reason RCE remains a well studied model problem (Bourdin et al., 2021; Goldblatt et al., 2013; Koll & Cronin, 2018; Popke et al., 2013; Seeley & Jeevanjee, 2021; Stevens & Bony, 2013; Wing et al., 2017), one which for reasons elegantly articulated by Polya (1962), is worth first understanding.

Konrad is equilibrated at prescribed values of T_s between 280 and 330 K with a fixed relative humidity RH = 80% (see Appendix for a more detailed model description). In contrast to earlier studies (Goldblatt et al., 2013; Koll & Cronin, 2018) we also performed simulations in which the temperature profile and heating rates are allowed to interact. This allows the tropopause temperature to evolve based on the radiative heating instead of setting it to a prescribed value. Although this has a quantitative effect on the feedback parameter, our simulations showed that the simpler approach, that those studies adopted, adequately captured the behavior in the more computationally demanding calculations. For this reason, we focus our attention on results developed using a fixed tropopause temperature of 175 K and an isothermal stratosphere. Figure 1a shows the resulting temperature profiles as a function of atmospheric pressure p.

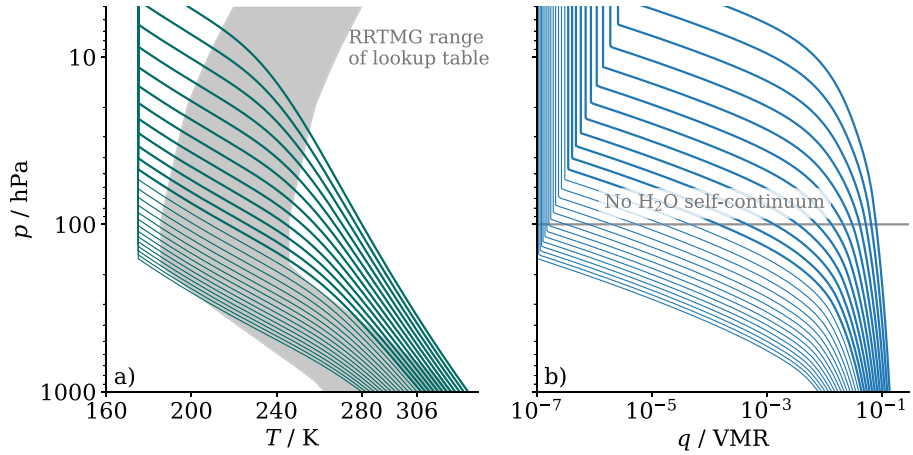

Figure 1. Equilibrium temperature (a) and water-vapor volume mixing ratio (b) profiles at different surface temperatures but constant CO_2 concentrations as a function of atmospheric pressure. The figure is clipped at 5 hPa to better visualize the troposphere. In addition, the rapid radiative transfer model for GCMs (RRTMG) reference temperature range, and the maximum (pressure) height up to which RRTMG considers the water-vapor continuum are shown.

The chosen relative humidity of 80% results in a moister troposphere compared to observations in the tropics, which often show a drying especially in the mid-troposphere, i.e., a C-shaped RH profile (Romps, 2014). As the emission window closes, changes in the strength of λ with warming are associated with water vapor progressively stealing ground on the flanks of the CO_2 lines (see Section 4). This behavior, because it depends on the overlap between the CO_2 and H_2O absorption, is also influenced by the chosen shape of the humidity profile (Bourdin et al., 2021), but not in ways that fundamentally influence our conclusions (see Supporting Information S1). In addition, some assumptions of the 1D-RCE framework presumably become less valid in extreme climates at $T_s \gg 310$. However, a detailed assessment of the general validity of the RCE framework is beyond the scope of this study, which is why we consider the same temperature range as existing studies (e.g., Meraner et al., 2013; Romps, 2020).

The RCE simulations are performed for CO_2 concentrations of 348 and 696 ppmv which allows us to compute the radiative forcing ΔF and the feedback parameter λ. We define ΔF at a given T_s as the difference in net radiation balance ΔN at the top of the atmosphere between these two CO_2 concentrations

$$\Delta F = \Delta N_{696\,\mathrm{ppmv}} - \Delta N_{348\,\mathrm{ppmv}} \tag{1}$$

The feedback parameter λ is defined as the change in ΔN between simulations at constant $CO_2 = 348$ ppmv and different T_s

$$\lambda(T_s) = \frac{\Delta N(T_s + \Delta T) - \Delta N(T_s - \Delta T)}{2\Delta T} \tag{2}$$

with surface temperature difference $\Delta T = 1$ K. Following our definition, a negative λ is associated with a stabilizing effect on the climate system. With this approach, we can study the temperature-dependence of the radiative forcing ΔF, the climate feedback λ, and the resulting climate sensitivity $S = -\Delta F/\lambda$. Note, that our definition of S does not account for changes in λ due to the doubling of the CO_2 concentration, which is usually included in estimates of S.

To check our method we have also performed simulations with a coupled T_s and computed λ as the regression of ΔN over ΔT_s during a perturbed simulation (Gregory et al., 2004). We find that the results are in very good agreement with those obtained using Equation 2. However, the strong temperature-dependence of λ makes the linear regression error-prone, which mostly manifests itself in spurious signals in the estimated effective forcing (y-intercept of the regression). Therefore, we opted for the well-established fixed-T_s approach.

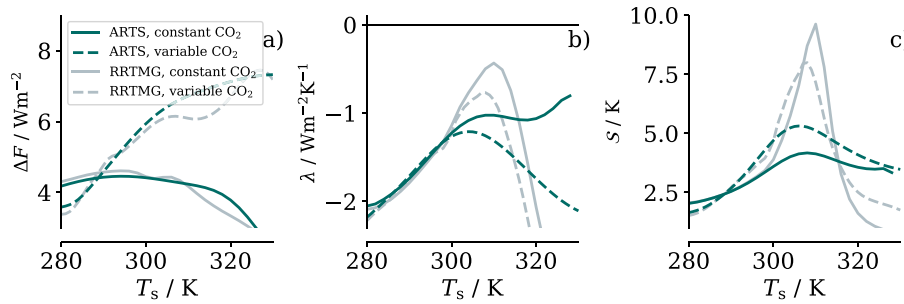

Figure 2. (a) Effective radiative forcing ΔF, (b) climate feedback parameter λ, and (c) equilibrium climate sensitivity S as function of surface temperature T_s. All quantities are shown for experiments using the radiation scheme rapid radiative transfer model for GCMs (RRTMG, gray) and the line-by-line radiative transfer model atmospheric radiative transfer simulator (ARTS, green). Solid lines represent simulations with a fixed CO_2 concentration of 348 ppmv, whereas for the dashed lines the CO_2 concentration was adjusted to ensure a constant outgoing-longwave radiation (following Romps, 2020).

Baseline simulations are performed using the Rapid Radiative Transfer Model for GCMs (RRTMG) (Mlawer et al., 1997). RRTMG is a fast radiation scheme which uses the correlated-k method with precalculated lookup tables for computational efficiency. For line-by-line simulations we replace the RRTMG longwave radiative transfer calculations with calculations using the Atmospheric Radiative Transfer Simulator (ARTS) (Buehler et al., 2018; Eriksson et al., 2011) which has been part of the Radiative Forcing Model Intercomparison Project (RFMIP, Pincus et al., 2020). In the chosen setup, ARTS represents the longwave radiative fluxes based on 32768 equidistant frequency points between 10 cm^{-1} and 3250 cm^{-1} ($\Delta\nu = 0.1$ cm^{-1}). Explicitly resolving the spectrum of OLR later allows us to investigate conceptual ideas about the dependence of OLR on T_s in different spectral regions.

For the sake of simplicity and to facilitate comparisons with previous modeling studies we do not consider the effects of ozone. We have performed calculations in which ozone is allowed to change, and while the basic physics that we describe are not influenced by this elaboration, as λ becomes small the effect of ozone can become important. Quantitatively its influence is found to depend on the details of its representation, particularly in light of the deepening of the troposphere with warming, an interesting issue that we are beginning to explore together with experts on ozone chemistry.

Further information about konrad's configuration, RRTMG, and ARTS is given in the Appendix.

3. Temperature-Dependence of the Feedback Parameter λ

We run konrad for T_s between 280 and 330 K to quantify the temperature-dependence of the feedback parameter

$$\lambda = f(T_s; I, \alpha, \mathrm{RH}, \chi) \tag{3}$$

with constant values of insolation I, surface albedo α, relative humidity RH, and the gaseous composition χ. Seeley and Jeevanjee (2021) consider the related problem $\lambda = f(T_s, CO_2; ...)$, where the CO_2 concentration is variable.

For low temperatures, calculations based on RRTMG and ARTS agree well with one another. Figure 2 (solid lines) shows the radiative forcing ΔF and the feedback parameter λ (as defined in Section 2), as well as the resulting equilibrium climate sensitivity S, as a function of T_s. Both results, using either RRTMG (gray) or the line-by-line radiative transfer model ARTS (green), show that λ (Figure 2b) increases from −2.1 to −1.3 W $m^{-2}K^{-1}$ as T_s increases from 280 to 300 K. A more detailed feedback analysis (not shown) identifies this increase with the temperature-dependence of the water-vapor feedback.

For $T_s > 300$ K, calculations with RRTMG result in a pronounced local maximum, or "bump", in S. This is seen in Figure 2c, where S increases from less than 3 K at $T_s = 300$ K to about 10 K at $T_s = 310$ K, and then rapidly decreases to less than 2 K at $T_s = 320$ K. Figure 2 further shows that RRTMG's response can

be attributed to changes of the feedback parameter λ, rather than the forcing. Hence the bump, and its origins, are similar to what was found in other studies (Meraner et al., 2013; Romps, 2020) using correlated-k radiative transfer. When using ARTS, however, λ does not decrease for $T_s > 305$ K. In contrast, after a local plateau around 305 K, λ begins to increase again at higher T_s. This is consistent with work by Goldblatt et al., 2013 (their Figure 4) who show that, at even higher T_s, water-vapor controls the emission in the whole OLR spectrum provoking a runaway greenhouse. Neither their study nor our results support the existence of a "bump" in clear-sky λ.

In addition, we performed another set of experiments with increased CO_2 concentrations (dashed lines in Figure 2) following the experimental setup by Romps (2020) and Seeley and Jeevanjee (2021). Using ARTS, we confirm the stabilizing effect of increased CO_2 concentrations as explained by the "radiator fins" described in Seeley and Jeevanjee (2021). However, simulations using RRTMG show the same qualitative behavior irrespective of the chosen CO_2 concentration. This strengthens our interpretation that the increase in λ as predicted by RRTMG has no physical explanation but is caused by inaccuracies in the treatment of radiative transfer.

RRTMG, and other fast-radiative transfer schemes, aggregate absorption features into bands, within which optical properties are calculated by interpolating across pre-computed look-up tables. This reduces the computational intensity and speeds up the calculations. In RRTMG the lookup tables are based on an assumed atmospheric composition and thermal structure, close to those of the present-day Earth (Mlawer et al., 1997, their Section 3.2). As it turns out, how one interprets the word "close" can be problematic. For instance, while RRTMG is documented to be valid for T_s as high as 320 K, this is based on a temperature profile representative of mid-latitude summer and assumes that there are no changes in the temperature lapse rate with increasing surface temperature (Mlawer et al., 1997, their Section 3.2). As a consequence, the temperature lapse-rate in the lookup table is larger than the moist-adiabat, which implies mid- and upper-tropospheric temperatures that are out of bounds at T_s above 306 K (see Figure 1a). Popp et al. (2015) attempted to minimize the resultant errors by extending the temperatures to acceptable bounds when performing the gaseous look-up. The look-up tables are only one source of error. Another, which we identified, arises from RRTMG's calculation of the water-vapor self continuum. For computational expediency this is fit to only two reference temperature values (at 260 and 296 K) and is neglected entirely for pressures less than 100 hPa. The latter becomes increasingly error prone as T_s increases above 296 K and the deepening troposphere causes a moistening above 100 hPa (see Figure 1b). For the case of RRTMG, these errors lead to an overestimation of OLR, which is misinterpreted as a decrease (more negative) of λ at high T_s. Coincidentally, this happens around the same temperature range at which the CO_2 mechanism described by Seeley and Jeevanjee (2021) begins to work.

In conclusion, using a line-by-line radiation model we find a robust increase of λ for T_s up to 330 K. Errors in the calculation of longwave irradiances by RRTMG are shown to be the cause of a spurious "bump" in clear-sky λ. This "bump" looks similar, but is entirely unrelated, to the local maximum in λ that Seeley and Jeevanjee (2021) find (and physically explain), when CO_2 is allowed to covary with T_s. For fixed CO_2, as T_s increases, λ increases, but remains more negative than -1 W m^{-2}K^{-1} even for temperatures as high as 330 K. At yet higher temperatures, and as reported by Goldblatt et al. (2013) for temperatures around 350 K, this negative feedback might completely vanish, albeit for a setup that is becoming increasingly artificial. Its substantially negative value for T_s as high as 330 K was less expected, something we address in more detail in the following section.

4. Spectral Analysis of λ and ΔF

To understand why λ is far from zero even at $T_s = 330$ K, we here examine the spectral feedback parameter λ_ν. This framework was used by Kluft et al. (2019) as well as Seeley and Jeevanjee (2021), and can also be used to study the role of different spectral regions in changing ΔF and S. The important difference between our situation, and the situation envisioned by Simpson (1928), is that H_2O is not the only absorber in the infrared. Were that the case it would not be possible to force the system by increasing atmospheric concentrations of CO_2. The problem as we pose it here, is not how Earth can respond to energy accumulated by an external process, such as insolation or accretion of extra-planetary material (Abe & Matsui, 1988;

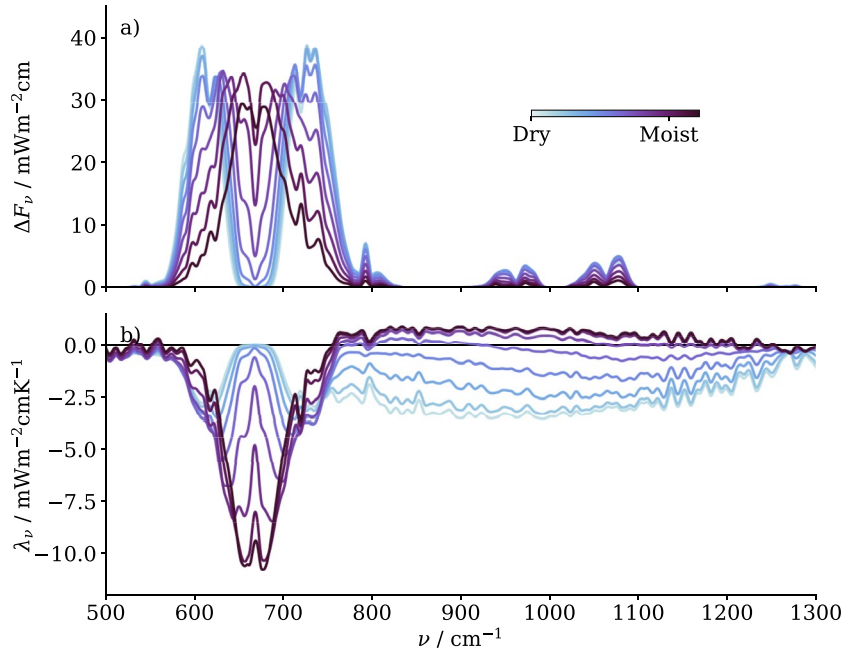

Figure 3. (a) Spectral radiative forcing ΔF_ν and (b) spectral feedback parameter λ_ν as functions of wavenumber ν. Darker shades of blue represent a warmer and moister atmosphere. The spectra are smoothed using a 15 cm^{-1} running mean and zoomed to a range of 500–1300 cm^{-1} to better resolve the CO_2 absorption band around 667 cm^{-1} and the atmospheric emission window between 715 and 1250 cm^{-1}. The actual line-by-line simulations cover a wavenumber range from 10 to 3250 cm^{-1}.

Kasting, 1988; Nakajima et al., 1992), but rather how the reduction of infrared irradiance of the atmosphere can be compensated through warming.

The spectral feedback parameter λ_ν can be derived from our line-by-line calculations using Equation 2. Figure 3b shows the smoothed λ_ν as a function of wavenumber ν for simulations at different temperatures (and hence absolute humidity). There is a strong temperature-dependence of λ_ν in the atmospheric window between 715 and 1,250 cm^{-1}. This is driven by the increasing water vapor concentration in the warming troposphere, as λ_ν is indeed close to zero as soon as the atmosphere becomes fully opaque at high temperatures (darker blue shades) and stays close to zero for higher T_s. Hence, our results link the findings of Koll and Cronin (2018) with the studies by Nakajima et al. (1992) and Goldblatt et al. (2013).

In our simulations the total λ remains negative for all T_s up to 330 K. We attribute this mainly to the thermal Planck feedback in the CO_2 bands around 667 cm^{-1}. Adopting the analogy introduced by Seeley and Jeevanjee (2021), the infrared emission attributable to tropospheric CO_2 acts as a spectral radiator fin, stabilizing the climate to greenhouse forcing. This effect, however, is limited by the water-vapor amount in the atmosphere: with increasing T_s, water-vapor controls an ever growing part of the emission spectrum. The deepening of the troposphere raises the emission level to lower pressure thereby reducing the impact of the CO_2 band (see Figure S3 in Supporting Information S1). Eventually, at T_s even higher than simulated in our study, it sets the emission temperature of the whole OLR resulting in a zero feedback. The value of T_s, at which this runaway greenhouse state is reached, depends on the relative humidity of the atmosphere. A subsaturated atmosphere column is stable at higher T_s (see Figure S1 in Supporting Information S1), which explains why our feedback is stable for even higher T_s than for the fully saturated simulations by Goldblatt et al. (2013).

Similar to the increase of λ we observe a reduction in ΔF with warming. Usually, the radiative forcing is thought to increase with T_s (Huang et al., 2016). Such an effect is apparent in our simulations, but only for lower values of T_s, up to 300 K (Figure 2a). This strengthening of ΔF with warming arises from a larger contribution from the band center (between 620 and 700 cm^{-1}). At higher T_s, ΔF decreases, so that with T_s = 320 K it is 18% less than its value at 295 K. The reduction in ΔF with warming is due to a weakening

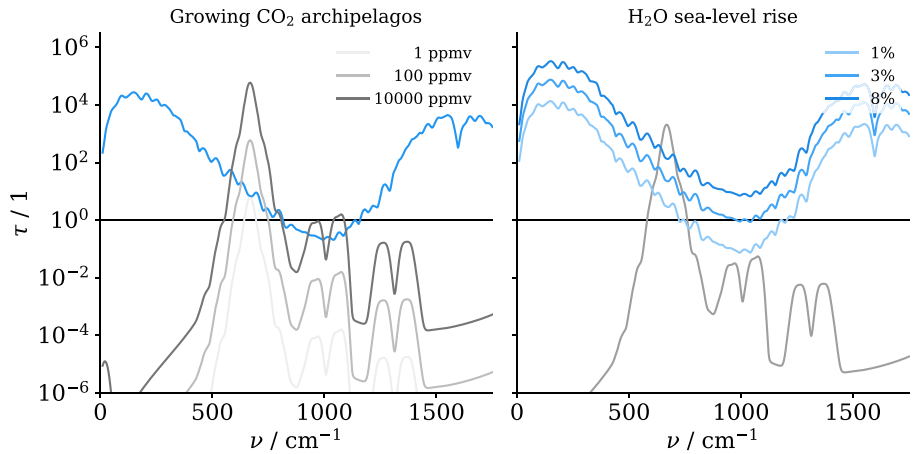

Figure 4. Optical thickness τ as a function of wavenumber ν. The left panel shows how the "CO_2 archipelagos" grow with an increase in atmospheric CO_2 concentration (darker greys). The right panel shows the rising "H_2O absorption sea-level" at higher water vapor volume mixing ratios (darker blues, the label states surface VMR while the actual humidity profile is computed based on a constant RH of 80%). In addition, the $\tau = 1$ line roughly indicates the location of opaque spectral regions ($\tau > 1$).

contribution from the edges of the 667 cm^{-1} CO_2 band (see Figure S2 in Supporting Information S1). At $T_s = 280$ K, 15% of the forcing is carried by the band center, at 320 K the forcing from the band center has increased more than threefold and is responsible for 60% of the total forcing.

CO_2 absorption is so strong near the central absorption feature, that emission to space from these wavelengths originates in the stratosphere. Only lines whose emission height resides in the troposphere, where temperatures decrease with height, contribute to reduced emissions—and hence forcing—from increasing CO_2 concentrations. As the tropopause rises with warming, an increasing fraction of the OLR originates from CO_2 in the troposphere, and its changes can contribute to the forcing. As increasing water vapor closes the window at $T_s > 300$ K, emission by H_2O increasingly dominates over emission by CO_2 on the flanks of the CO_2 band. This reduces the contribution of tropospheric CO_2 to the OLR, thereby reducing the contribution of its changes to forcing. The latter increasingly dominates at warmer temperatures, weakening ΔF from a doubling of CO_2 by about 18% (from a value around 4.5 to 3.7 Wm^{-2} for T_s increasing from 280 to 320 K), consistent with an analytical model of the CO_2 forcing by Jeevanjee et al. (2020). Our analysis identifies the same mechanism—the increasing dominance of water-vapor over the OLR—to affect both λ and ΔF in opposite ways, albeit with very different impact.

Seeley and Jeevanjee (2021) demonstrated how an increase in CO_2 concentration strengthens the CO_2 absorption band in the atmospheric window: at some point the CO_2 replaces H_2O as the dominant absorber and acts as a "CO_2 radiator fin". To understand the effects of warming on both λ and ΔF we find a different analogy helpful. We picture a "CO_2 archipelago in a developing, and eventually rising, sea of water-vapor absorption" (see Figure 4, the poetically inclined might think of these as Planckian outcroppings in a Simpsonian sea). From this point of view the share of the radiation that is emitted to space by H_2O in the troposphere, versus that from tropospheric CO_2 or from the surface, determines the strength of both λ and ΔF. As CO_2 concentrations rise, or the troposphere deepens, the CO_2 archipelago gains prominence—new islands even appear with rising CO_2 concentrations, as seen in Seeley and Jeevanjee (2021)—increasing the magnitude of both ΔF and λ. Warming of the atmosphere leads to the development of a "sea of absorption," which progressively reclaims the spectral landscape from CO_2 and the surface. This reduces ΔF for a given increase in CO_2 and progressively masks the ability of radiation from the "sea-floor" to escape to space. In our simulations, at $T_s = 320$ K the "absorption sea-level" is so completely determined by temperature, as envisaged by Simpson (1928), that the net radiative response to warming in the window region, 715 cm^{-1} $< \nu <$ 1250 cm^{-1}, completely vanishes. At this point only the tallest mountains of the "CO_2 archipelago", whose prominence is pronounced due to a rising tropopause, are left to balance an increase in forcing.

5. Discussion and Conclusions

We perform calculations using the 1D-RCE model konrad at different surface temperatures T_s to analyze the temperature-dependence of the feedback parameter λ for fixed and variable CO_2 concentrations. A line-by-line treatment of longwave radiant energy transfer (ARTS) is used to ensure an accurate computation of radiative fluxes and heating rates over a wide temperature range. By comparison to calculations with the RRTMG radiation scheme, we find that the use of the latter (albeit faster) scheme leads to increasingly erroneous results as surface temperatures increase beyond 300 K–errors in climate sensitivity are larger than a factor of two at 310 K. This is within the range of temperatures sampled by models with very high climate sensitivities subject to quadrupling of atmospheric CO_2. The erroneous behavior leads to a local maximum (or "bump") in the clear-sky climate sensitivity. Coincidentally, a similar "bump" is predicted by the "CO_2 radiator fin" mechanism by Seeley and Jeevanjee (2021), which arises from the strengthening of the Planck feedback from more pronounced CO_2 absorption features. Using two different sets of simulations, we show that RRTMG computes the "bump" irrespective of the CO_2 concentration. The resulting unphysical trend in climate sensitivity looks similar to what has been found in at least two other modeling studies (e.g., Meraner et al., 2013; Romps, 2020) using this same, or a similar, treatment of radiative transfer. In Romps (2020) both effects, the large increases in CO_2, which the climate sensitivity also depends on, and the RRTMG errors are conflated. However, our simulations suggest that the erroneous treatment of radiative transfer alone is sufficient to cause the reversing trend in climate sensitivity.

Using ARTS and a constant CO_2 concentration, λ increases from -2.1 to -1.0 $\mathrm{W\,m^{-2}\,K^{-1}}$ for T_s between 280 and 330 K, which can be attributed to a progressive masking of the Planck feedback by increased water vapor absorption in the atmospheric window as well as at the wings of the CO_2 band. For $T_s > 300$ K the radiative forcing ΔF due to CO_2-doubling decreases by about 18% from a value around 4.5–3.7 $\mathrm{W\,m^{-2}}$. A spectral analysis of the radiative forcing reveals that this decrease is also caused by increased water-vapor absorption which masks the radiative forcing at the flanks of the CO_2 absorption band. To help conceptualize these effects we propose the picture of "CO_2 archipelagos in a sea of water-vapor absorption" to describe the subtle trial of strength between CO_2 and water-vapor absorption. This picture leads to the surprising result that as the atmosphere transitions to a moist greenhouse, CO_2 not only becomes less effective as a forcer, its presence and relative abundance compared to H_2O also becomes a prerequisite for maintaining a negative atmospheric feedback.

Appendix A

Appendix A1: Model Configuration

We are using the 1D radiative-concective equilibrium model konrad (Kluft et al., 2021, v0.8.1). The boundary conditions are following Kluft et al. (2019) with a CO_2 concentration of 348 ppmv. The solar constant is set to 551.58 $\mathrm{W\,m^{-2}}$ at a zenith angle of 42.05° resulting in an insolation of 409.6 $\mathrm{W\,m^{-2}}$ (Cronin, 2014; Wing et al., 2017). The relative humidity in the troposphere is set to 80% to ensure a reasonable amount of humidity in the upper troposphere, which is key for the interaction of lapse-rate and water-vapor feedbacks (Kluft et al., 2019; Minschwaner & Dessler, 2004). Above the cold-point tropopause the volume mixing ratio is kept constant.

Appendix A2: Convective Adjustment

Konrad uses a hard convective adjustment to the moist-adiatic temperature profile. In practice, after each iteration, the tropospheric temperatures are set to follow the moist-adiabat from the surface temperature up to the top-of-convection, which is defined as the level at which the radiative cooling switches to heating. The use of a moist adiabat is an idealization, that only approximately holds in present-day conditions, and there is a possibility that the atmosphere might deviate further from it in a warmer climate. However, were one to extent our findings to more realistic atmosphere, this would not be the first assumption we would recommend relaxing, more interesting effects are likely to be caused by other gases (especially ozone) and clouds.

Appendix A3: Radiation Scheme

We are using the Rapid Radiative Transfer Model for GCMs (RRTMG, Mlawer et al., 1997) through the CliMT Python package. We have checked the radiative fluxes computed with CliMT-RRTMG and a standalone version and find that they agree within 1%. RRTMG is a rapid radiation scheme and uses the distributed-k method for computational efficiency. This method requires precalculated lookup tables that are designed to span a wide range of atmospheric states.

Appendix A4: Line-by-Line Treatment of Radiation

We are using the Atmospheric Radiative Transfer Simulator (ARTS) (Buehler et al., 2018; Eriksson et al., 2011). ARTS is a line-by-line radiative transfer model and is used to calculate the longwave radiative fluxes using four emission angles (streams) and based on 32768 equidistant frequency points between 10 and 3,250 cm^{-1} ($\Delta\nu = 0.1$ cm^{-1}). Gas absorption is based on the HITRAN database for gas species (Gordon et al., 2017) and additionally the MT_CKD model (Mlawer et al., 2012) for the continuum absorption of water vapor, CO_2, molecular nitrogen (all Version 2.52), and oxygen (Version 1.00).

Data Availability Statement

Open Research Primary data is available on Zenodo through https://doi.org/10.5281/zenodo.4565189. Konrad v0.9.4 is available at https://doi.org/10.5281/zenodo.5607058, and the latest development version can be found at github.com/atmtools/konrad.

Acknowledgments
The research is supported by public funding to the Max Planck Society and through the European Union's Horizon 2020 Research and Innovation programs (Grant 820829, to the CONSTRAIN Project). With this work we contribute to the Cluster of Excellence "CLICCS—Climate, Climatic Change, and Society" (EXC 2037; Project Number 390683824), and to the Center for Earth System Research and Sustainability (CEN) of Universität Hamburg. The authors would like to thank the ARTS community. Open access funding enabled and organized by Projekt DEAL.

References

Abe, Y., & Matsui, T. (1988). Evolution of an impact-generated H_2O–CO_2 atmosphere and formation of a hot proto-ocean on Earth. *Journal of the Atmospheric Sciences*, *45*(21), 30812–33101. https://doi.org/10.1175/1520-0469(1988)045{3081:EOAIGHi}2.0.CO;2

Andrews, T. (2014). Using an AGCM to diagnose historical effective radiative forcing and mechanisms of recent decadal climate change. *Journal of Climate*, *27*(3), 1193–1209. https://doi.org/10.1175/JCLI-D-13-00336.1

Bourdin, S., Kluft, L., & Stevens, B. (2021). Dependence of climate sensitivity on the given distribution of relative humidity. *Geophysical Research Letters*, *48*(8), e2021GL092462. https://doi.org/10.1029/2021gl092462

Buehler, S. A., Mendrok, J., Eriksson, P., Perrin, A., Larsson, R., & Lemke, O. (2018). ARTS, the atmospheric radiative transfer simulator—version 2.2, the planetary toolbox edition. *Geoscientific Model Development*, *11*(4), 1537–1556. https://doi.org/10.5194/gmd-11-1537-2018

Charney, J. G., Arakawa, A., Baker, D. J., Bolin, B., Dickinson, R. E., Goody, R. M., & Wunsch, C. I. (1979). *Carbon dioxide and climate: A scientific assessment*. (Tech. Rep.).

Cronin, T. W. (2014). On the choice of average solar zenith angle. *Journal of the Atmospheric Sciences*, *71*(8), 2994–3003. https://doi.org/10.1175/JAS-D-13-0392.1

Dacie, S., Kluft, L., Schmidt, H., Stevens, B., Buehler, S. A., Nowack, P. J., et al. (2019). A 1D RCE study of factors affecting the tropical tropopause layer and surface climate. *Journal of Climate*, *32*(20), 6769–6782. https://doi.org/10.1175/JCLI-D-18-0778.1

Eriksson, P., Buehler, S. A., Davis, C. P., Emde, C., & Lemke, O. (2011). ARTS, the atmospheric radiative transfer simulator, version 2. *Journal of Quantitative Spectroscopy and Radiative Transfer*, *112*(10), 1551–1558. https://doi.org/10.1016/j.jqsrt.2011.03.001

Goldblatt, C., Kavanagh, L., & Dewey, M. (2017). The palaeoclimate and terrestrial exoplanet radiative transfer model intercomparison project (PALAEOTRIP): Experimental design and protocols. *Geoscientific Model Development*, *10*(11), 3931–3940. https://doi.org/10.5194/gmd-10-3931-2017

Goldblatt, C., Robinson, T. D., Zahnle, K. J., & Crisp, D. (2013). Low simulated radiation limit for runaway greenhouse climates. *Nature Geoscience*, *6*(8), 661–667. https://doi.org/10.1038/ngeo1892

Gordon, I. E., Rothman, S., Hill, C., Kochanov, R. V., Tan, Y., Bernath, P. F., et al. (2017). The HITRAN2016 molecular spectroscopic database. *Journal of Quantitative Spectroscopy and Radiative Transfer*, *203*, 3–69. https://doi.org/10.1016/j.jqsrt.2017.06.038

Gregory, J. M., & Andrews, T. (2016). Variation in climate sensitivity and feedback parameters during the historical period. *Geophysical Research Letters*, *43*(8), 3911–3920. https://doi.org/10.1002/2016GL068406

Gregory, J. M., Ingram, W. J., Palmer, M. A., Jones, G. S., Stott, P. A., Thorpe, R. B., & Williams, K. D. (2004). A new method for diagnosing radiative forcing and climate sensitivity. *Geophysical Research Letters*, *31*(3), 1–4. https://doi.org/10.1029/2003GL018747

Huang, Y., Tan, X., & Xia, Y. (2016). Inhomogeneous radiative forcing of homogeneous greenhouse gases. *Journal of Geophysical Research: Atmosphere*, *121*(6), 2780–2789. https://doi.org/10.1002/2015JD024569

Ingram, W. (2010). A very simple model for the water vapour feedback on climate change. *Quarterly Journal of the Royal Meteorological Society*, *136*(646), 30–40. https://doi.org/10.1002/qj.546

Jeevanjee, N., Seeley, J., Paynter, D., & Fueglistaler, S. (2020). An analytical model for CO_2 forcing, Part II: State-dependence and spatial variations. *Earth and Space Science Open Archive*, *47*. https://doi.org/10.1002/essoar.10503404.1

Kasting, J. F. (1988). Runaway and moist greenhouse atmospheres and the evolution of Earth and Venus. *Icarus*, *74*(3), 472–494. https://doi.org/10.1016/0019-1035(88)90116-9

Kluft, L., Dacie, S., & Bourdin, S. (2021). *The possibility to perturb the relative humidity distribution*. https://doi.org/10.5281/zenodo.4434837

Kluft, L., Dacie, S., Buehler, S. A., Schmidt, H., & Stevens, B. (2019). Re-examining the first climate models: Climate sensitivity of a modern radiative-convective equilibrium model. *Journal of Climate*, *32*(23), 8111–8125. https://doi.org/10.1175/JCLI-D-18-0774.1

Koll, D. D. B., & Cronin, T. W. (2018). Earth's outgoing longwave radiation linear due to H_2O greenhouse effect. *Proceedings of the National Academy of Sciences*, *115*(41), 10293–10298. https://doi.org/10.1073/pnas.1809868115

Kutzbach, J. E., He, F., Vavrus, S. J., & Ruddiman, W. F. (2013). The dependence of equilibrium climate sensitivity on climate state: Applications to studies of climates colder than present. *Geophysical Research Letters*, *40*(14), 3721–3726. https://doi.org/10.1002/grl.50724

Manabe, S., & Bryan, K. (1985). CO_2-induced change in a coupled ocean-atmosphere model and its paleoclimatic implications. *Journal of Geophysical Research*, *90*(C6), 11689–11707. https://doi.org/10.1029/JC090iC06p11689

Meraner, K., Mauritsen, T., & Voigt, A. (2013). Robust increase in equilibrium climate sensitivity under global warming. *Geophysical Research Letters*, *40*(22), 5944–5948. https://doi.org/10.1002/2013GL058118

Minschwaner, K., & Dessler, A. E. (2004). Water vapor feedback in the tropical upper troposphere: Model results and observations. *Journal of Climate*, *17*, 12722–21282. https://doi.org/10.1175/1520-0442(2004)017<1272:WVFITT>2.0.CO;2

Mlawer, E. J., Payne, V. H., Moncet, J.-L., Delamere, J. S., Alvarado1, M. J., & Tobin, D. C. (2012). Development and recent evaluation of the MT_CKD model of continuum absorption. *Philosophical Transactions of the Royal Society A*, *370*, 2520–2556. https://doi.org/10.1098/rsta.2011.0295

Mlawer, E. J., Taubman, S. J., Brown, P. D., Iacono, M. J., & Clough, S. A. (1997). Radiative transfer for inhomogeneous atmospheres: RRTM, a validated correlated-k model for the longwave. *Journal of Geophysical Research*, *102*, 16663–16682. https://doi.org/10.1029/97jd00237

Nakajima, S., Hayashi, Y., & Abe, Y. (1992). A study on the "Runaway Greenhouse Effect" with a one-dimensional radiative–convective equilibrium model. *Journal of the Atmospheric Sciences*, *492*(23), 2256–2266. https://doi.org/10.1175/1520-0469(1992)049<2256:asotge>2.0.co;2

Pincus, R., Buehler, S. A., Brath, M., Crevoisier, C., Jamil, O., Franklin Evans, K., & Tellier, Y. (2020). Benchmark calculations of radiative forcing by greenhouse gases. *Journal of Geophysical Research: Atmosphere*, *125*(23), e2020JD033483. https://doi.org/10.1029/2020jd033483

Polya, G. (1962). *How to solve it*. Princeton University Press.

Popke, D., Stevens, B., & Voigt, A. (2013). Climate and climate change in a radiative-convective equilibrium version of ECHAM6. *Journal of Advances in Modeling Earth Systems*, *5*(1), 1–14. https://doi.org/10.1029/2012MS000191

Popp, M., Schmidt, H., & Marotzke, J. (2015). Initiation of a runaway greenhouse in a cloudy column. *Journal of the Atmospheric Sciences*, *72*(1), 452–471. https://doi.org/10.1175/JAS-D-13-047.1

Popp, M., Schmidt, H., & Marotzke, J. (2016). Transition to a moist greenhouse with CO_2 and solar forcing. *Nature Communications*, *7*(1), 1–10. https://doi.org/10.1364/acpc.2016.ath3k.1

Romps, D. M. (2014). An Analytical Model for Tropical Relative Humidity. *Journal of Climate*, *27*(19), 7432–7449. https://doi.org/10.1175/JCLI-D-14-00255.1

Romps, D. M. (2020). Climate sensitivity and the direct effect of carbon dioxide in a limited-area cloud-resolving model. *Journal of Climate*, *33*(9), 3413–3429. https://doi.org/10.1175/JCLI-D-19-0682.1

Schneider, T., Kaul, C. M., & Pressel, K. G. (2019). Possible climate transitions from breakup of stratocumulus decks under greenhouse warming. *Nature Geoscience*, *12*(3), 163–167. https://doi.org/10.1038/s41561-019-0310-1

Seeley, J. T., & Jeevanjee, N. (2021). H_2O windows and CO_2 radiator fins: A clear-sky explanation for the peak in equilibrium climate sensitivity. *Geophysical Research Letters*, *48*(4), e2020GL089609. https://doi.org/10.1029/2020gl089609

Simpson, S. G. C. (1928). *Some studies in terrestrial radiation*. Edward Stanford.

Stevens, B., & Bony, S. (2013). Water in the atmosphere. *Physics Today*, *66*(6), 29–34. https://doi.org/10.1063/PT.3.2009

Wing, A. A., Reed, K. A., Satoh, M., Stevens, B., Bony, S., & Ohno, T. (2017). Radiative-convective equilibrium model intercomparison project. *Geoscientific Model Development Discussions*, 1–34. https://doi.org/10.5194/gmd-2017-213

Wolf, E. T., & Toon, O. B. (2015). The evolution of habitable climates under the brightening sun. *Journal of Geophysical Research: Atmosphere*, *120*(12), 5775–5794. https://doi.org/10.1002/2015jd023302